Molecular Therapy
Methods & Clinical Development
Original Article

AAV-mediated BMP7 gene therapy counteracts insulin resistance and obesity

Estefania Casana,[1,2,3,4] Veronica Jimenez,[1,2,3,4] Claudia Jambrina,[1,2,3] Victor Sacristan,[1,2] Sergio Muñoz,[1,2,3] Jordi Rodo,[1,2] Ignasi Grass,[1,2] Miquel Garcia,[1,2,3] Cristina Mallol,[1,2] Xavier León,[1,2,3] Alba Casellas,[1,2,3] Víctor Sánchez,[1,2] Sylvie Franckhauser,[1,2,3] Tura Ferré,[1,2,3] Sara Marcó,[1,2,3] and Fatima Bosch[1,2,3]

[1]Center of Animal Biotechnology and Gene Therapy (CBATEG), Universitat Autònoma de Barcelona, 08193 Bellaterra, Barcelona, Spain; [2]Department of Biochemistry and Molecular Biology, Universitat Autònoma de Barcelona, 08193 Bellaterra, Barcelona, Spain; [3]CIBER de Diabetes y Enfermedades Metabólicas Asociadas (CIBERDEM), 28029 Madrid, Spain

Type 2 diabetes, insulin resistance, and obesity are strongly associated and are a major health problem worldwide. Obesity largely results from a sustained imbalance between energy intake and expenditure. Therapeutic approaches targeting metabolic rate may counteract body weight gain and insulin resistance. Bone morphogenic protein 7 (BMP7) has proven to enhance energy expenditure by inducing non-shivering thermogenesis in short-term studies in mice treated with the recombinant protein or adenoviral vectors encoding *BMP7*. To achieve long-term BMP7 effects, the use of adeno-associated viral (AAV) vectors would provide sustained production of the protein after a single administration. Here, we demonstrated that treatment of high-fat-diet-fed mice and ob/ob mice with liver-directed AAV-BMP7 vectors enabled a long-lasting increase in circulating levels of this factor. This rise in BMP7 concentration induced browning of white adipose tissue (WAT) and activation of brown adipose tissue, which enhanced energy expenditure, and reversed WAT hypertrophy, hepatic steatosis, and WAT and liver inflammation, ultimately resulting in normalization of body weight and insulin resistance. This study highlights the potential of AAV-BMP7-mediated gene therapy for the treatment of insulin resistance, type 2 diabetes, and obesity.

INTRODUCTION

Type 2 diabetes (T2D) has become a major health problem because of its alarmingly growing prevalence worldwide. Obesity is very strongly associated with insulin resistance and T2D. These diseases lead to long-term damage, dysfunction, and failure of several key organs, resulting in a variety of severe complications such as hepatosteatosis, non-alcoholic steatohepatitis (NASH), arthritis, hypertension, cardiovascular disease, retinopathy, nephropathy, or neurodegeneration, among others.[1–5] Although conventional pharmacologic treatments and lifestyle intervention have proven effective for many obese and T2D patients, these approaches are not successful in all cases and could result in undesirable side effects. Therefore, there is an urgent need for novel therapeutic approaches to prevent and reverse the T2D and obesity epidemic.

The continued imbalance between energy intake and expenditure is the main cause of obesity. In obese individuals, adipose tissue hypertrophy is associated with accumulation of fat in ectopic compartments, such as the liver, and in development of insulin resistance. Increased energy expenditure, through non-shivering thermogenesis mediated by brown adipose tissue (BAT) uncoupling activity and/or browning (appearance of beige adipocytes) of subcutaneous white adipose tissue (WAT), has been associated with leanness and improved insulin sensitivity in both obese animal models and humans.[6–12]

The bone morphogenetic protein (BMP) family belongs to the transforming growth factor β (TGF-β) superfamily of cytokines that regulate an array of fundamental cellular processes including proliferation, differentiation, apoptosis and morphogenesis.[13,14] Bone morphogenic protein 7 (BMP7) has also been described as promoting white adipogenesis, brown adipocyte differentiation, and thermogenesis.[15,16] Administration of recombinant BMP7 or adenoviral (Ad) vectors encoding *BMP7* to healthy or high-fat diet (HFD)-fed mice increases whole-body energy expenditure in short-term studies.[16–18] Moreover, these treatments also improve insulin sensitivity and reverse obesity in HFD-fed, ob/ob, and db/db mice.[18,19] Nevertheless, periodic administration of recombinant BMP7 protein is required,[19] which, in addition, could compromise treatment compliance by patients. Likewise, the use of Ad-BMP7 vectors is not able to promote long-term expression of the transgene due to the high immunogenicity of Ad vectors.[20,21]

Here, we hypothesized that adeno-associated viral (AAV) vector-mediated gene therapy offers the possibility of a one-time treatment that would lead to sustained production of BMP7 for extended periods of time with low toxicity and immunogenicity.[22,23] In this study,

Received 7 July 2021; accepted 13 March 2022;
https://doi.org/10.1016/j.omtm.2022.03.007.

[4]These authors contributed equally

Correspondence: Fatima Bosch, Center of Animal Biotechnology and Gene Therapy Edifici H, Universitat Autònoma de Barcelona 08193 Bellaterra, Barcelona, Spain.
E-mail: fatima.bosch@uab.es

we found that treatment of obese HFD-fed or ob/ob mice with AAV vectors encoding *Bmp7* under the control of a liver-specific promoter induced browning of subcutaneous WAT and activation of BAT, which increased energy expenditure and mediated long-term reversal of body weight gain and insulin resistance. These results highlight the potential of AAV-BMP7-mediated gene therapy for the treatment of T2D and obesity.

RESULTS

Liver-specific BMP7 overexpression mediates persistent reversion of obesity

To determine the anti-obesogenic and anti-insulin resistance effects of AAV-BMP7-mediated gene therapy, 2-month-old C57BL/6 mice were first fed with either chow or an HFD for 6 weeks. During this period, the weight of chow- and HFD-fed animals increased by 19% and 53%, respectively (Figure 1A). Chow-fed and obese HFD-fed animals were then treated intravenously (i.v.) with 1×10^{12} vg of AAV vectors of serotype 8 encoding an optimized murine BMP7 coding sequence (om*Bmp7*) under the control of a synthetic hybrid liver-specific promoter composed of three copies of the hepatocyte control region (HCR) enhancer from the apolipoprotein E gene (ApoE) and the human α1-antitrypsin (hAAT) promoter (AAV-BMP7). As controls, another cohort of obese HFD-fed mice and the cohort of chow-fed mice received the same dose of non-coding AAV8 null vectors (AAV-null). Following AAV delivery, mice were maintained on chow or HFD feeding for about 6 months, and body weight and metabolic parameters were monitored regularly.

Chow-fed animals treated with AAV-BMP7 maintained their body weight at the time of AAV treatment, which was slightly lower than that of chow-fed AAV-null-treated mice, which progressively gained weight as the animals aged (Figure 1A). HFD-fed animals treated with AAV-BMP7 vectors experienced progressive loss of body weight following gene delivery, which stabilized within a few weeks to a weight similar to that of chow-fed AAV-BMP7-treated mice (Figures 1A and S1A). This was parallel to normalization of the weight of the liver and the main adipose depots of HFD-fed AAV-BMP7-treated animals compared with the HFD-fed null-treated mice (Figures 1B and S1B–S1H). Moreover, the weight of the main white and brown fat pads of chow- and HFD-fed AAV-BMP7-treated animals was slightly lower than that of chow-fed null-treated mice (Figures 1B and S1B–S1G).

The decrease in body weight was parallel to increased circulating BMP7 levels (Figure 1C). In HFD-fed AAV-BMP7-treated mice, serum BMP7 concentration was very high 4 weeks after AAV administration and gradually decreased, reaching levels similar to those of chow-fed AAV-BMP7-treated mice at week 23 post-AAV (Figure 1C). A similar serum BMP7 level profile was observed in chow-fed AAV-BMP7-treated mice (Figure 1C). The changes in BMP7 circulating levels would be consistent with increased expression of BMP7 from the synthetic HCR/hAAT promoter under conditions of high hepatic fat content, such as liver steatosis after HFD feeding. In this regard, transcription from the ApoE promoter has already been reported to be induced in the liver after high-fat and/or high-cholesterol feeding in different species, including mice, rat, guinea pig, rabbit, and cow.[24–28] In agreement, the lean-chow-fed animals at 4 and 12 weeks after treatment with AAV-BMP7 showed circulating levels much lower than HFD-fed AAV-BMP7-treated mice (Figure 1C). As body and liver weight normalized, serum BMP7 concentration also decreased in HFD-fed AAV-BMP7-treated mice, reaching levels similar to those of chow-fed AAV-BMP7-treated mice at the end of the study (Figure 1C). No alteration in the liver damage marker alanine aminotransferase (ALT) was observed at any time after AAV-BMP7 treatment (Figure 1D). In contrast, HFD-fed mice administered AAV-null vectors showed progressively very high serum ALT levels (Figure 1D) in agreement with increased adiposity in the liver (Figure 1B).

Because of the hAAT promoter, AAV-BMP7-treated mice showed specific overexpression of codon-optimized BMP7 in the liver, which resulted in increased hepatic BMP7 content (Figures 1E and S1I). This agreed with the increased transduction of the liver by AAV8 vectors (Figure S1J). In contrast, marginal levels of endogenous *Bmp7* expression, compared with the expression of om*Bmp7*, were observed in all the tissues examined, including the kidney, the main endogenous producer of the factor[29] (Figures 1F and 1G).

AAV-BMP7 reverses HFD-associated WAT hypertrophy and inflammation

HFD feeding induced an increase in the size of white adipocytes in null-treated mice (Figures 2A and 2B). In agreement with decreased adiposity, morphometric analysis of visceral (epididymal, eWAT) and subcutaneous (inguinal, iWAT) WAT revealed that the area of white adipocytes of BMP7-treated animals was similar to that of animals fed a chow diet (Figures 2A and 2B). As a result of the reversion of WAT hypertrophy, serum adiponectin and leptin levels were normalized in HFD-fed mice treated with AAV-BMP7 vectors (Figures 2C and 2D).

Obesity also causes inflammation of WAT.[30] Immunostaining of eWAT sections for the macrophage-specific marker Mac2 revealed increased presence of "crown-like" structures in HFD-fed null-treated mice, while HFD-fed animals treated with AAV-BMP7 had no sign of macrophage infiltration (Figures 2E and 2F). This was parallel to the normalization of the expression of the macrophage markers *Cd68* and *F4/80* in BMP7-treated mice (Figure 2E), indicating that BMP7 expression counteracted the inflammation of WAT associated with obesity.

BMP7 downstream signaling was assessed in WAT by evaluating the phosphorylation levels of SMAD1/5/8 (pSMAD1/5/8) and p38 mitogen-activated protein kinase (MAPK) (p-p38MAPK), which are downstream effectors of the canonical and non-canonical, respectively, BMP7 signaling pathways.[31,32] Increased pSMAD1/5/8 and unchanged p-p38MAPK were observed in eWAT of HFD-fed AAV-BMP7-treated mice (Figures 2G and 2H). These observations agreed with previous studies reporting BMP7-mediated increased pSMAD1/5/8 in white preadipocytes but a lack of enhancement of p-p38MAPK in the 3T3-L1 cell line.[16]

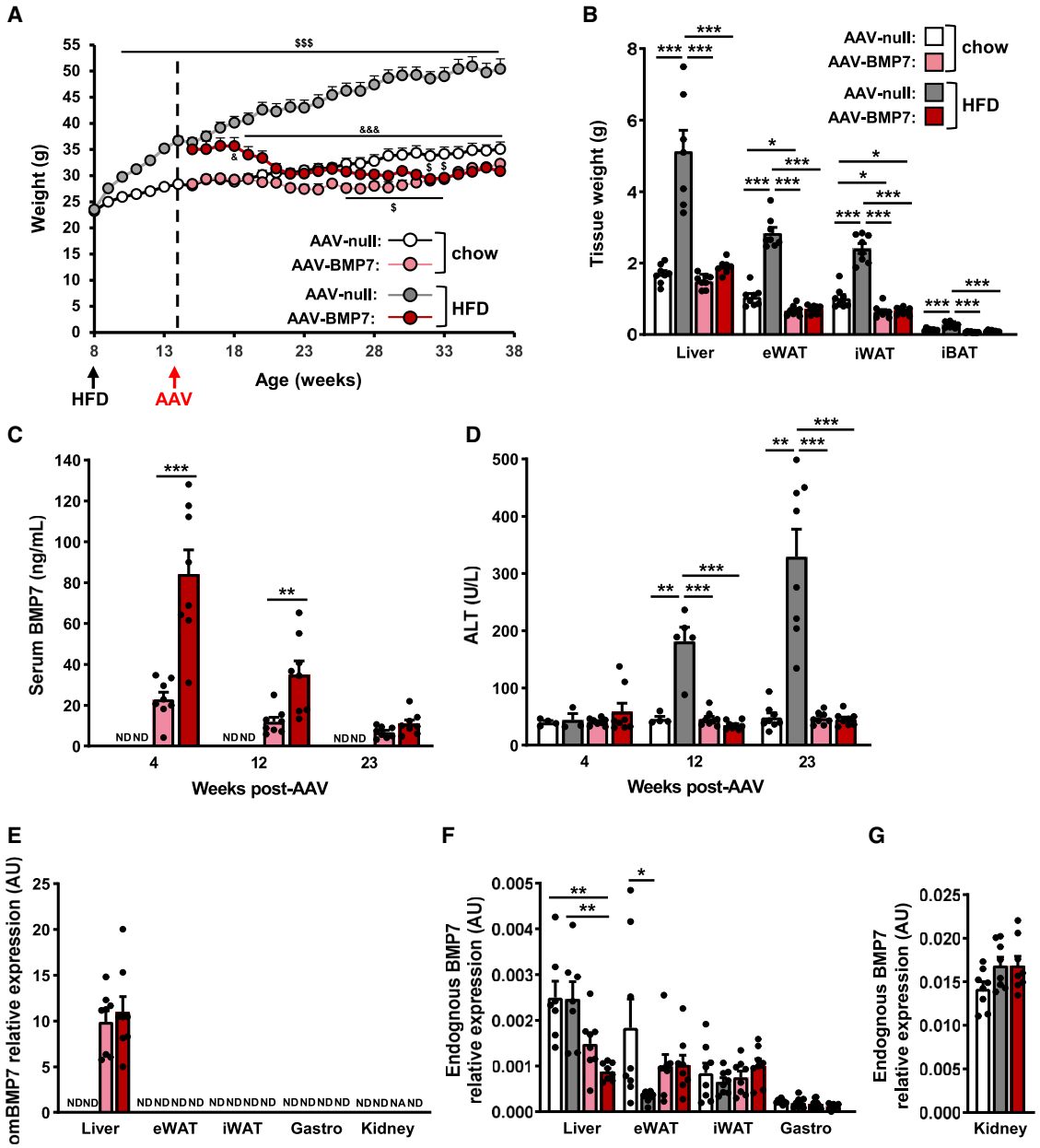

Figure 1. AAV-mediated liver gene transfer of BMP7 counteracts HFD-induced obesity

(A) Body-weight follow-up of C57BL/6 mice fed either chow or an HFD for 6 weeks and then administered intravenously with 1×10^{12} vg of AAV-BMP7 vector per mouse. Control obese mice and control chow-fed mice were treated with AAV-null vectors (n = 8/group). $^{\&}p < 0.05$ and $^{\&\&\&}p < 0.001$ versus the HFD-fed null-injected group. $^{\$}p < 0.05$ and $^{\$\$\$}p < 0.001$ versus the chow-fed null-injected group. (B) Weight of the liver, epididymal (eWAT) and inguinal (iWAT) white adipose tissue depots, and interscapular brown adipose tissue (iBAT) of the same cohorts as in (A) (n = 7–8/group). (C) Circulating levels of BMP7 (n = 8/group). (D) Alanine aminotransferase (ALT) serum levels (n = 3–8/group). (E) Quantitative PCR analysis of *Bmp7* expression in the liver, eWAT, iWAT, gastrocnemius, and kidney was performed with primers that specifically detected vector-derived BMP7 mRNA (omBMP7) (n = 7–8/group). (F) Quantitative PCR analysis of endogenous *Bmp7* expression in liver, eWAT, iWAT, and gastrocnemius (n = 7–8/group). (G) Quantitative PCR analysis of endogenous *Bmp7* expression in kidney (n = 8/group). All values are expressed as the mean ± SEM. ND, not detected; NA, not available; AU, arbitrary units; HFD, high-fat diet. *p < 0.05, **p < 0.01, and ***p < 0.001.

Treatment with AAV-BMP7 enhances energy expenditure

To elucidate the mechanism(s) underlying the counteraction of obesity in HFD-fed mice treated with AAV-BMP7, food intake and energy expenditure were evaluated. Weekly measurements of the number of calories consumed per day revealed that the energy intake of HFD-fed BMP7-treated animals was slightly reduced (about 12%)

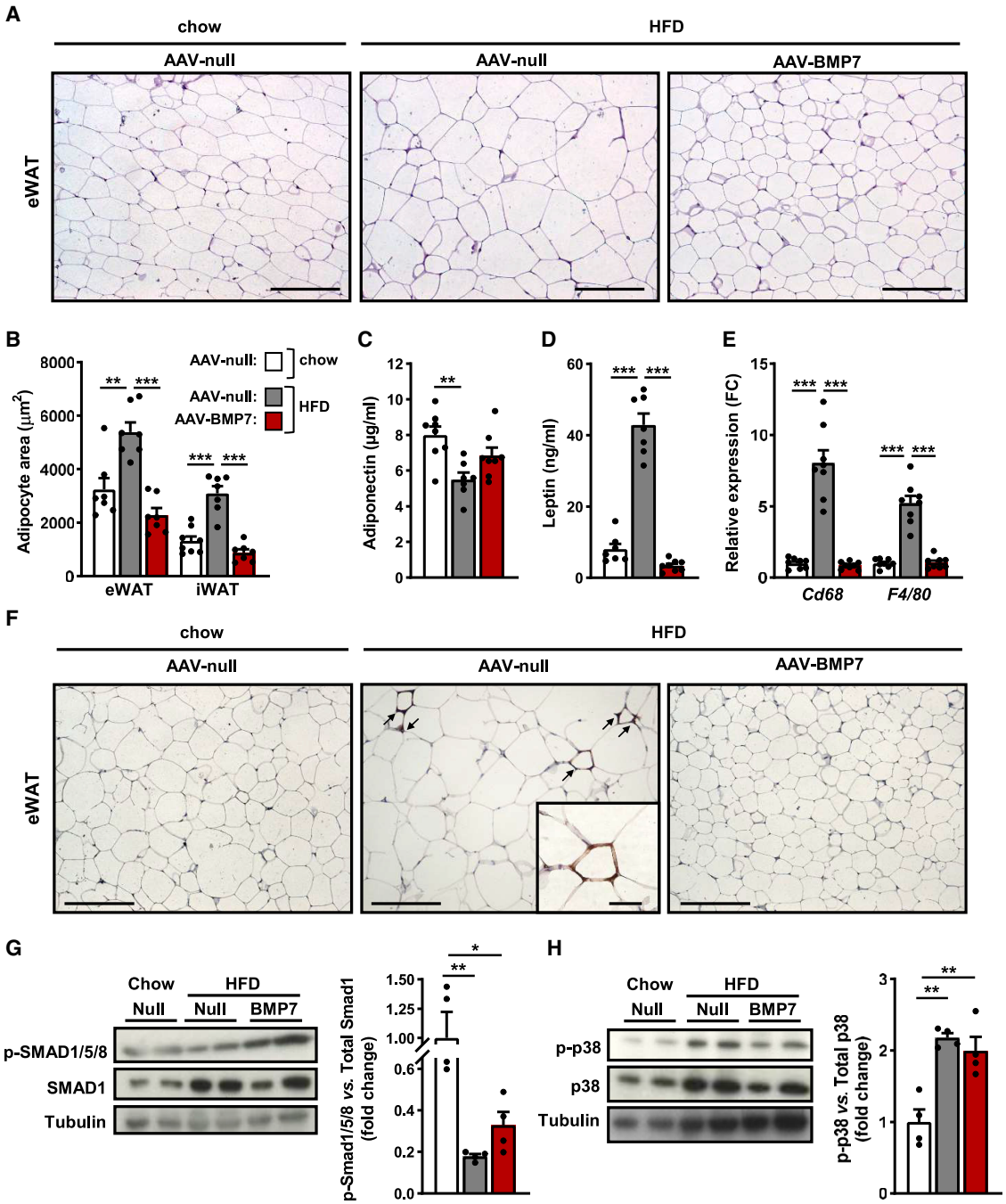

Figure 2. Reversal of WAT hypertrophy and inflammation by AAV-BMP7 treatment

(A) Representative images of hematoxylin-eosin staining of eWAT. Scale bars: 200 μm. (B) Morphometric analysis of the area of eWAT and iWAT adipocytes (n = 7–8/group). (C and D) Circulating levels of adiponectin (C) and leptin (D) (n = 7–8/group). (E) Quantitative PCR analysis of the expression of the macrophage markers *Cd68* and *F4/80* in eWAT (n = 8/group). (F) Immunohistochemistry for the macrophage-specific marker Mac2 in eWAT sections. Scale bars: 200 and 50 μm (inset). (G) Determination of phosphorylated SMAD1/5/8 (p-SMAD1/5/8) protein abundance in eWAT: immunoblot and densitometric analysis (n = 4/group). (H) Determination of phosphorylated p38 (p-p38) protein abundance in eWAT: immunoblot and densitometric analysis (n = 4/group). All values are expressed as the mean ± SEM. HFD, high-fat diet; FC, fold change. *p < 0.05, **p < 0.01, and ***p < 0.001.

compared with that of the HFD-fed null-treated cohort (Figures 3A and S2A). Nevertheless, normalization of food intake data per body weight revealed that HFD-fed mice treated with AAV-BMP7 ate more than the chow-fed counterparts (Figure 3B). When indirect calorimetry was performed 10 weeks after AAV delivery, BMP7-treated mice had higher oxygen consumption and energy expenditure during both the light and the dark cycles than HFD-fed null control counterparts (Figures 3C, S2B, and S2C). No striking differences in spontaneous activity or respiratory exchange ratio were observed among groups (Figures S2D and S2E).

To evaluate whether non-shivering thermogenesis was responsible for the enhancement of energy expenditure, the degree of activation of BAT and browning of subcutaneous iWAT was assessed. Compared with HFD-fed null-treated mice, AAV-BMP7-treated mice showed decreased lipid deposition in iBAT and the presence of numerous multilocular adipocytes in iWAT (Figure 3D). This was parallel to increased expression of the thermogenic markers *Ucp1*, *Cidea*, and *Ppargc1a* in iWAT of AAV-BMP7-treated mice (Figures 3E and 3F). No changes in the expression of *Ucp1* and *Cidea* were detected in the iBAT of these mice, although other thermogenic markers such as *Ppargc1a*, *Dio2*, and *Elovl3* were upregulated (Figure S2F), in agreement with BAT activation.

AAV-BMP7 ameliorates hepatic steatosis and counteracts insulin resistance

As expected, HFD-fed null-treated animals showed marked hepatic steatosis, which was ameliorated after treatment with AAV-BMP7 vectors (Figure 4A). This finding was parallel to a reduction in total hepatic triglyceride content and a decrease in macrophage infiltration, evidenced by the lower number of $Mac2^{+}$ cells in liver sections (Figures 4A and 4B). Moreover, the expression of the pro-inflammatory cytokines *Ifnγ*, *Mcp1*, *Ccl5*, and *Tnf1α* was normalized in AAV-BMP7-treated HFD-fed mice (Figure 4C). In agreement with normalization of hepatic steatosis, serum cholesterol levels were also normalized (Figure S3A).

Obese HFD-fed null-treated mice showed normal fed and fasted glycemia (Figure 4D) but were hyperinsulinemic (Figure 4E). In contrast, HFD-fed AAV-BMP7-treated mice were normoglycemic and normoinsulinemic (Figures 4D and 4E). To evaluate whole-body insulin sensitivity of AAV-BMP7-treated animals, intraperitoneal insulin tolerance tests (ITTs) were performed 1.5 and 4 months post-AAV delivery. Feeding with HFD led to insulin resistance in animals receiving AAV-null vectors, while treatment with AAV-BMP7 counteracted HFD-induced insulin resistance (Figures 4F and S3B). Moreover, HFD-fed AAV-treated mice showed higher insulin sensitivity than chow-fed mice receiving null vectors (Figures 4F and S3B), indicating that AAV-BMP7 treatment was able to counteract insulin resistance. Moreover, similar to chow-fed mice, HFD-fed animals treated with AAV-BMP7 vectors showed increased glucose tolerance compared with the null-treated obese cohort (Figures 4G and S3C). These results were parallel to increased *Glut4* expression in eWAT and iWAT of HFD-fed AAV-BMP7-treated mice, suggesting increased glucose uptake in both visceral and subcutaneous WAT that likely contributed to increased insulin sensitivity and glucose tolerance (Figure S3D).

Treatment of ob/ob mice with AAV-BMP7

To further evaluate the anti-obesogenic and anti-insulin resistance effects of AAV-mediated BMP7 gene transfer, ob/ob mice were used, since they are a well-known model of extreme obesity and insulin resistance.[33] Eleven-week-old ob/ob mice were treated i.v. with 1×10^{13} vg AAV-BMP7 vectors. As controls, AAV-null vectors were administered to another cohort of ob/ob animals. Whereas the body weight of null-injected ob/ob mice increased as animals aged, the body weight of ob/ob animals treated with AAV-BMP7 progressively decreased after AAV administration (Figure 5A). These changes resulted from increased circulating levels of BMP7 (Figure 5B). As expected, AAV-BMP7 treatment led to overexpression of codon-optimized *Bmp7* specifically in the liver, increased hepatic BMP7 content, and high hepatic transduction by AAV8 vectors (Figures 5C, 5D, and S4A). Endogenous *Bmp7* expression was mainly detected in kidney, although at marginal levels (Figure S4B). In agreement with reduced body weight, the weight of the fat pads was decreased in ob/ob BMP7-treated animals (Figures 5E and S4C). Moreover, animals treated with AAV-BMP7 vectors showed reduced size of white adipocytes in eWAT and iWAT (Figure 5F). These findings were associated with a marked increase in serum adiponectin levels (Figure 5G). In addition, we observed increased pSMAD1/5/8 and unchanged p-p38MAPK in eWAT of AAV-BMP7-treated ob/ob mice (Figures S4D and S4E).

The decreased adiposity may result, at least in part, from the reduced food intake observed in AAV-BMP7-treated ob/ob mice (Figures 5H, S4F, and S4G). In contrast to HFD-fed AAV-BMP7-treated mice, ob/ob mice treated with AAV-BMP7 vectors showed neither marked reduction of lipid accumulation in BAT nor multilocular adipocytes in iWAT (Figure 5F). However, expression of *Ucp1* and *Elov3* was upregulated in both iWAT and iBAT (Figures 5I–5L). Moreover, increased *Ppargc1a* expression levels were also observed in iBAT (Figure 5M). These results suggested induction of non-shivering thermogenesis in AAV-BMP7-treated ob/ob mice.

Control ob/ob mice presented marked hepatic steatosis, whereas treatment with AAV-BMP7 significantly decreased liver weight and hepatic lipid accumulation (Figures 6A–6C). ob/ob mice treated with AAV-BMP7 also exhibited markedly reduced expression of pro-inflammatory cytokines in the liver (Figure 6D). ob/ob animals treated with AAV-BMP7 showed similar fed glycemia but markedly decreased fed insulinemia (Figures 6E and 6F). Treatment with AAV-BMP7 improved insulin sensitivity in comparison with AAV-null-treated ob/ob mice (Figure 6G), confirming the anti-insulin resistance effects of AAV-BMP7 observed in HFD-fed animals. BMP7 has been reported to induce hepatic insulin signaling in obese mice via inhibition of MAPKs and induction of phosphorylation of GSK3β (p-GSK3β).[34] In agreement, ob/ob mice treated with AAV-BMP7 showed increased p-GSK3β and reduced p-p38MAPK in the

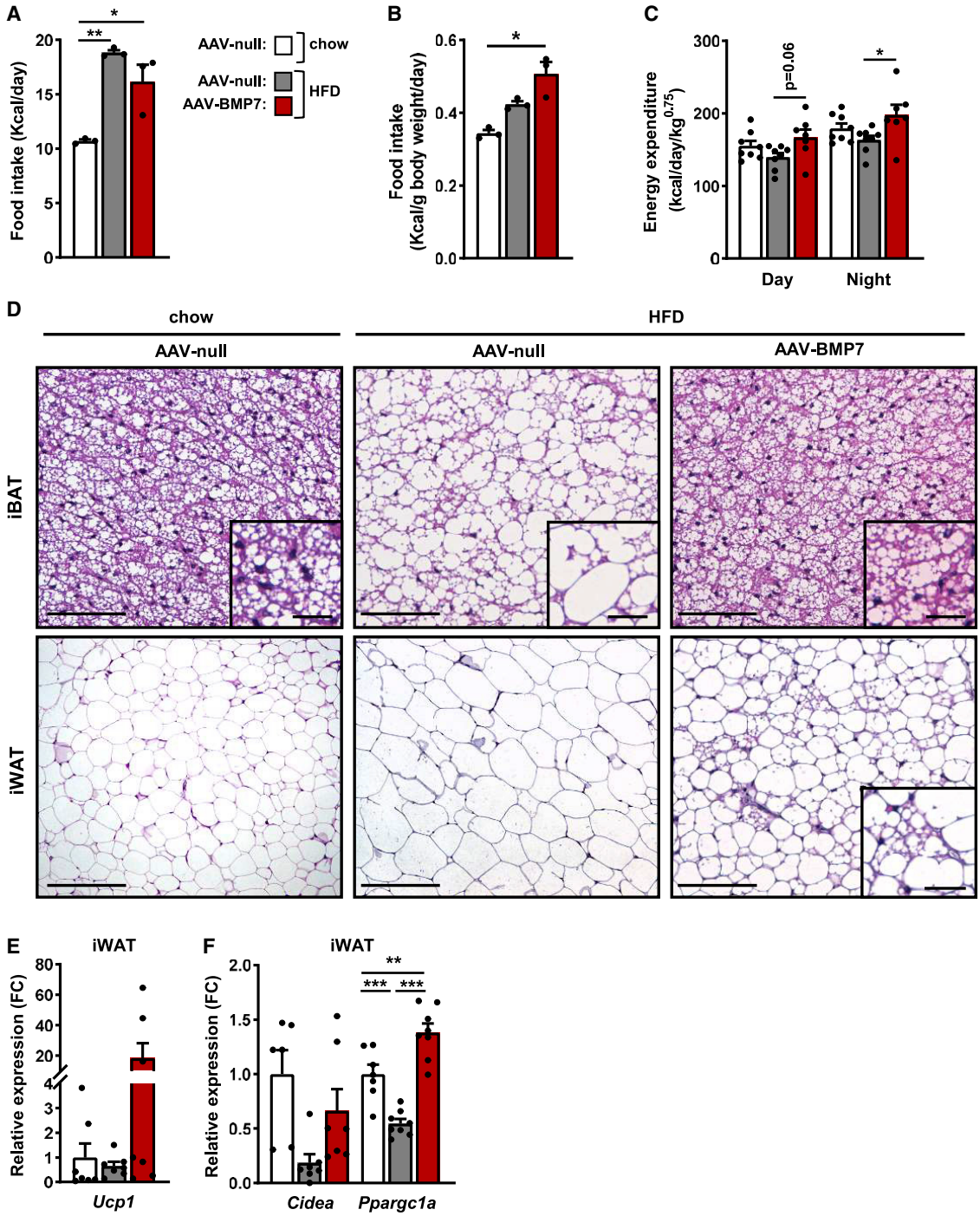

Figure 3. AAV-BMP7 increases energy expenditure, decreases fat accumulation in iBAT and iWAT, and induces browning

(A) Histogram depicting the mean food intake per day from week 15 to week 36 of age of HFD-fed mice treated with either AAV-BMP7 or AAV-null vectors and of chow-fed mice administered AAV-null vectors (n = 3 cages/group and 2–3 mice/cage). (B) Food intake normalized by body weight from week 15 to week 36 of age (n = 3 cages/group and 2–3 mice/cage). (C) Energy expenditure was measured with an indirect open-circuit calorimeter 10 weeks after AAV vector delivery. Data were taken during the light and dark cycles (n = 7–8/group). (D) Hematoxylin-eosin staining of iBAT and iWAT sections. Scale bars: 200 and 50 μm (inset). (E and F) Quantitative PCR analysis in iWAT of the expression of the thermogenic markers *Ucp1* (E) and *Cidea* and *Ppargc1a* (F) (n = 6–8/group). All values are expressed as the mean ± SEM. HFD, high-fat diet; FC, fold change. *p < 0.05, **p < 0.01, and ***p < 0.001.

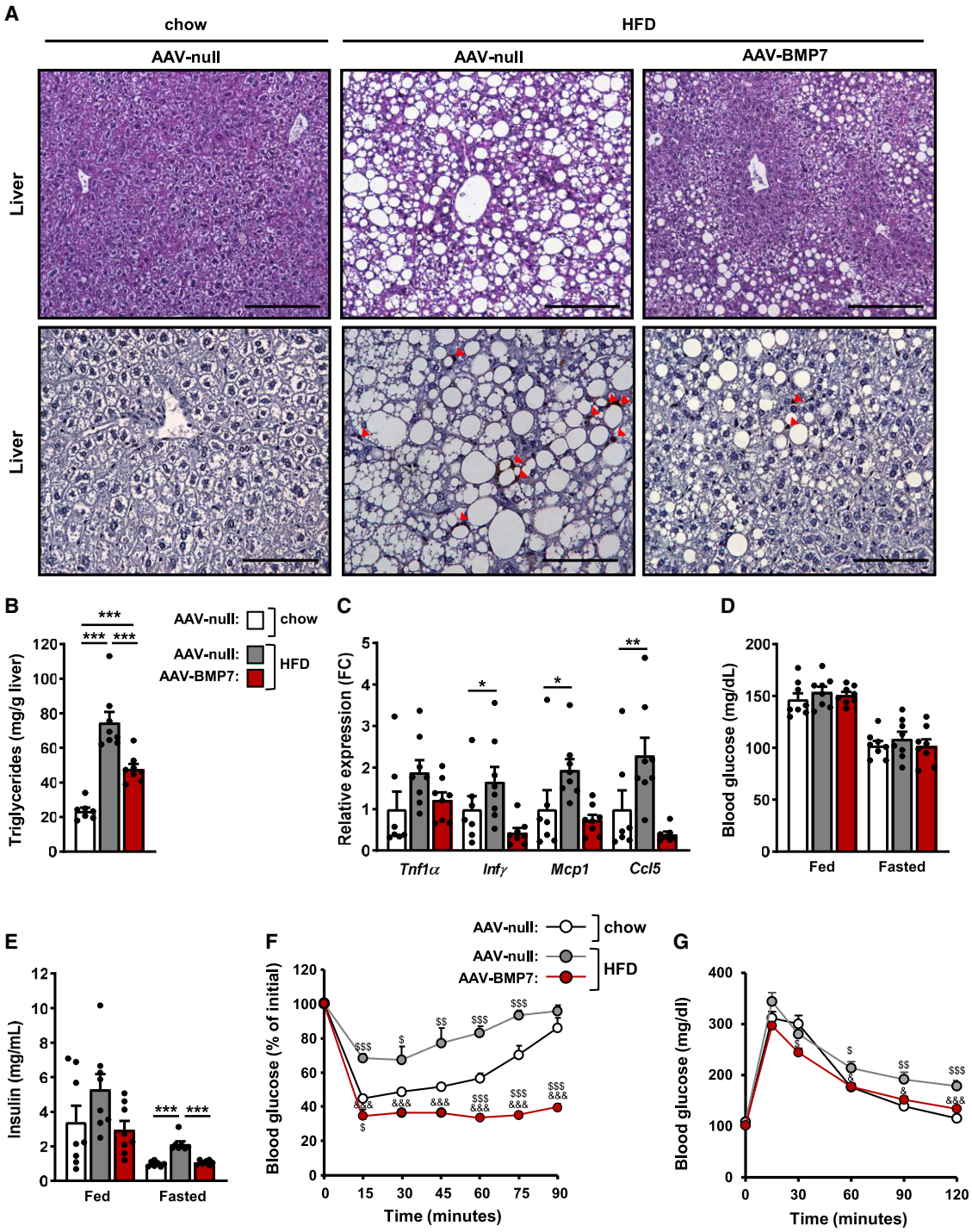

Figure 4. Treatment with BMP7-encoding vectors improves hepatic steatosis and reverses insulin resistance

(A) Hematoxylin-eosin staining (top) and immunostaining for the macrophage-specific marker Mac2 (bottom) of liver sections. Red arrows indicate macrophages. Scale bars: 200 μm (hematoxylin-eosin) and 100 μm (Mac2). (B) Hepatic triglyceride content (n = 7–8/group). (C) Quantitative PCR analysis of the expression of the pro-inflammatory cytokines *Tnfα*, *Ifnγ*, *Mcp1*, and *Ccl5* in the liver (n = 7–8/group). (D) Fed and fasted blood glucose levels 19 and 8 weeks after vector administration, respectively (n = 8/group). (E) Fed and fasted serum insulin levels 19 and 20 weeks after vector delivery, respectively (n = 7–8/group). (F) Insulin sensitivity was determined after an

(legend continued on next page)

liver (Figures 6H and 6I). These findings suggested that p-GSK3β and p-p38MAPK would be involved in the AAV-BMP7-mediated improvement of insulin resistance.

DISCUSSION

In this study, increased liver-derived BMP7 circulating levels increased energy expenditure, normalized WAT hypertrophy and inflammation, and reversed hepatic steatosis and inflammation, which in turn counteracted obesity and insulin resistance. We proved disease reversal in HFD-fed mice, the model that most closely resembles the metabolic characteristics of human obesity and insulin resistance.[35] The efficacy of AAV-mediated BMP7 gene transfer to the liver was further confirmed in the genetically obese ob/ob mouse model. AAV-BMP7 treatment elicited superior anti-insulin resistance and anti-obesogenic therapeutic benefit in comparison with previous studies using Ad-BMP7 vectors or periodic administration of recombinant BMP7 protein.[16–19] Recombinant BMP7 or Ad-BMP7 prevented or partially reduced body weight gain and improved insulin sensitivity in HFD-fed, ob/ob, and db/db mice, but failed to fully counteract obesity and insulin resistance.[17–19] While these studies demonstrated therapeutic benefit for 2–4 weeks,[16–19] one-time administration of AAV-BMP7 vectors resulted in long-lasting metabolic efficacy in agreement with lack of immunogenicity of AAV vectors.[22,23]

The present study in male mice represents a proof of concept of the beneficial effects of liver-directed AAV-BMP7-mediated gene therapy to counteract obesity and insulin resistance. Transduction of the liver by AAV vectors has been widely reported to be markedly decreased in female mice in comparison with male mice.[36–45] This phenomenon is not restricted to a particular AAV vector serotype.[36–44] This sexual dimorphism has been proved to be independent of the promoter and mouse strain used[36,37,46] and seems to be androgen driven.[36] In contrast to the results obtained in rodent models, studies performed in non-human primates have revealed similar levels of AAV-mediated liver transduction in male and female animals.[47,48]

To achieve therapeutic efficacy in obesity and insulin resistance, in the present study, we treated HFD-fed mice with 1×10^{12} vg of AAV8-hAAT-BMP7 vector per mouse. This dose efficiently mediated high BMP7 secretion into the circulation (Figure 1C), which led to a reversal of body weight gain and augmented insulin sensitivity. Nevertheless, previous studies in our laboratory have demonstrated that higher circulating levels of a therapeutic factor are required in ob/ob mice to mediate similar therapeutic efficacy compared with that elicited in HFD-fed mice.[49] Therefore, ob/ob mice were treated with a dose of AAV-BMP7 vectors 10-fold higher than that used in HFD-fed mice. ob/ob mice treated with 1×10^{13} vg of AAV8-hAAT-BMP7 per mouse showed markedly decreased body weight and improved insulin sensitivity.

AAV-BMP7-mediated reversal of obesity probably resulted from increased non-shivering thermogenesis in both BAT and subcutaneous WAT leading to enhanced energy expenditure. Similarly, BAT activation was described in lean and obese mice treated with recombinant BMP7 or Ad-BMP7 vectors.[16,17] BMP7 has also been reported to upregulate thermogenesis in adipocytes derived from human BAT.[50] Increased expression of UCP1 and multilocular beige adipocytes were also detected in iWAT of C57BL/6J mice treated with recombinant BMP7.[17] In addition, murine and human adipogenic precursor cells from subcutaneous WAT have been reported to differentiate into brown-like adipocytes upon stimulation with BMP7 *in vitro*.[51,52] Nevertheless, our results highlighted differences in BMP7-mediated induction of browning between HFD-fed C57BL/6 mice and ob/ob mice, which lacked multilocular adipocytes in subcutaneous WAT, although this tissue did overexpress thermogenic markers. The propensity for browning varies among mouse strains,[53] and browning differences between HFD-fed C57BL/6 and ob/ob mice have previously been described during intermittent fasting, in which HFD-fed C57BL/6 but not ob/ob mice exhibited beige adipocytes in WAT.[54–56] Moreover, strains of mice that have a higher propensity for browning show a greater degree of protection from diet-induced obesity.[57] Likewise, browning of WAT has been described to play a more important role than BAT activation in promoting weight loss in mice after cold or β-adrenergic stimulation.[58] In humans, it has been described that BAT comprises both brown and beige adipocytes,[59–61] and browning of WAT has also been documented in human adults.[62–64]

AAV-mediated gene transfer of *Bmp4*, another member of the BMP family, to the liver of chow-diet-fed mice or mice treated with AAV-BMP4 prior to HFD feeding also led to browning of subcutaneous WAT and increased whole-body energy expenditure.[65] Nevertheless, in already obese HFD-fed mice, AAV-mediated genetic engineering of the liver with BMP4 failed to enhance browning of adipose tissue or to reverse obesity.[66] BMP4 resistance in WAT of obese HFD-fed mice has been suggested as the underlying cause of this lack of therapeutic efficacy.[65,67] In this regard, increased mRNA levels of endogenous *Bmp4* were detected in subcutaneous WAT of obese HFD-fed mice compared with lean animals.[65,67] Moreover, increased gene and protein expression of a BMP4 antagonist and decreased BMP4 downstream signaling in subcutaneous WAT were also reported.[65,67] Similar results have been documented in human adipocytes from subcutaneous WAT of obese patients.[68] BMP4 has also been reported to be secreted by adipocytes[68], which may be consistent with the increased serum BMP4 levels observed in HFD-fed and db/db mice[19] as well as obese humans.[69–71] In contrast, age-dependent decreased circulating BMP7 levels have been reported in HFD-fed and db/db mice.[19] Moreover, we found that the expression levels of endogenous *Bmp7* were similar in iWAT of chow- and HFD-fed

intraperitoneal injection of insulin (0.75 units insulin/kg body weight) 17 weeks post-AAV delivery. Results were calculated as the percentage of initial blood glucose levels (n = 8, chow AAV-null; n = 8, HFD AAV-null; and n = 7, HFD AAV-BMP7). (G) Glucose tolerance was performed 8 weeks post-AAV (1 g glucose/kg body weight) (n = 8/group). Fasted refers to 16 h of food deprivation. All values are expressed as the mean ± SEM. HFD, high-fat diet; FC, fold change. $^{*}p < 0.05$, $^{**}p < 0.01$, and $^{***}p < 0.001$. $^{\&}p < 0.05$ and $^{\&\&\&}p < 0.001$ versus the HFD-fed null-injected group. $^{\$}p < 0.05$, $^{\$\$}p < 0.01$, and $^{\$\$\$}p < 0.001$ versus the chow-fed null-injected group.

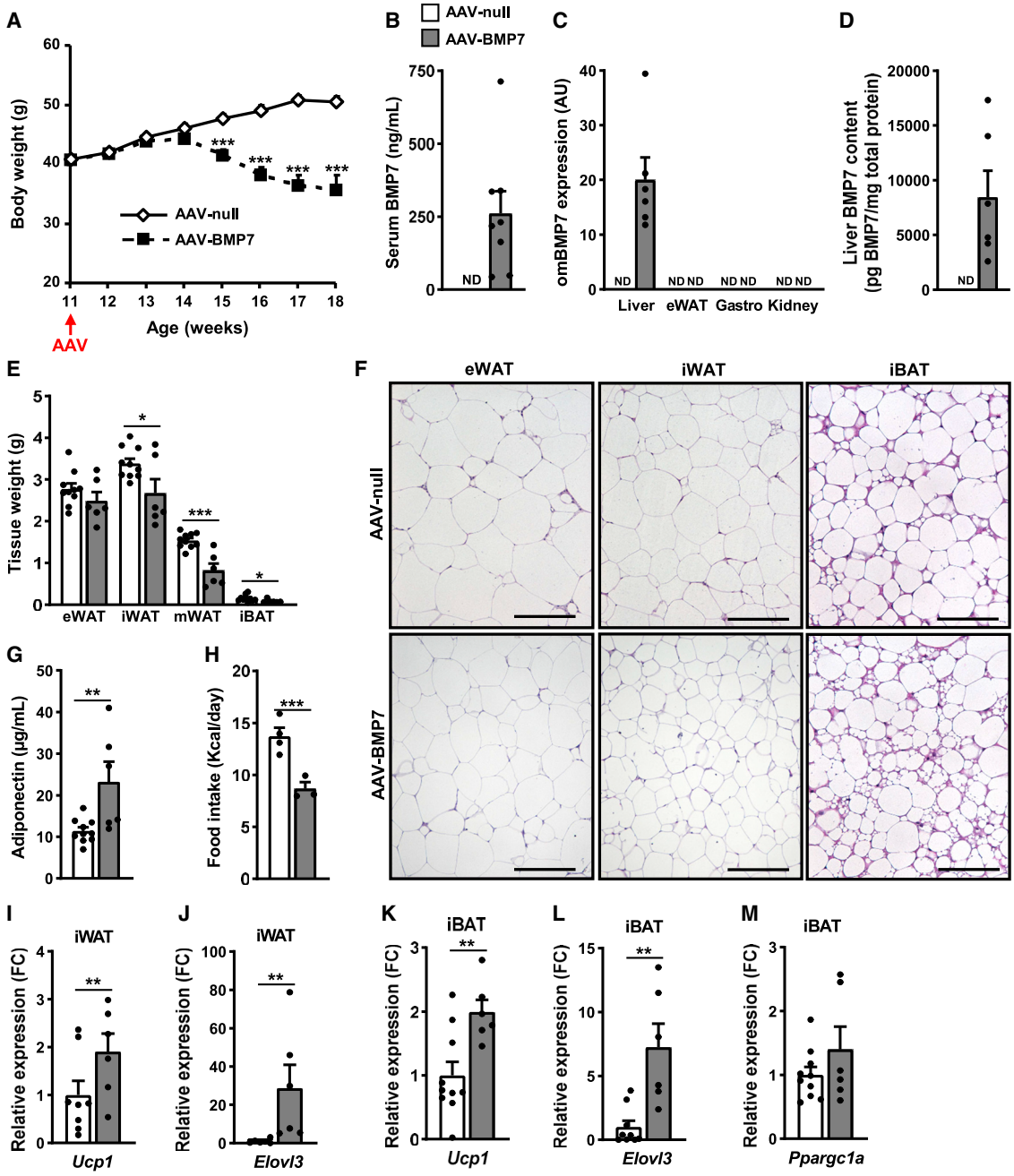

Figure 5. Reduced obesity in ob/ob mice treated with AAV-BMP7 vectors. ob/ob mice were administered intravenously with 1 × 10^{13} vg of either AAV-BMP7 or AAV-null vector per mouse and followed up for 7 weeks

(A) Follow-up of the body weight (n = 10, AAV-null, and n = 9, AAV-BMP7). (B) Serum BMP7 levels at 7 weeks after vector administration (n = 8–10/group). (C) Quantitative PCR analysis of om*BMP7* expression in the liver, eWAT, gastrocnemius (Gastro), and kidney. The qPCR was performed with primers that specifically detected vector-derived BMP7 mRNA (om*BMP7*) (n = 6–10/group). (D) Liver BMP7 content 7 weeks after vector administration (n = 6–10/group). (E) Weight of the eWAT, iWAT, mesenteric white adipose tissue (mWAT), and iBAT (n = 6–10/group). (F) Representative images of the hematoxylin-eosin staining of eWAT, iWAT, and iBAT tissue sections obtained from ob/ob animals injected with either null or BMP7-encoding AAV. Scale bars: 100 µm. (G) Serum adiponectin levels (n = 6–10/group). (H) Histogram depicting the mean food intake per day from week 13 to week 17 of age of ob/ob mice treated with either AAV-BMP7 or AAV-null vectors (n = 4 cages, AAV-null; n = 3 cages, AAV-BMP7; 1–3 mice/cage). (I–M) Quantitative PCR analysis in iWAT (I, J) or iBAT (K, L, M) of the expression of the thermogenic markers *Ucp1* (I, K), *Elovl3* (J, L), or *Ppargc1a* (M) (n = 6–10/group). All values are expressed as the mean ± SEM. ND, not detected; FC, fold change; AU, arbitrary units. *p < 0.05, **p < 0.01, and ***p < 0.001.

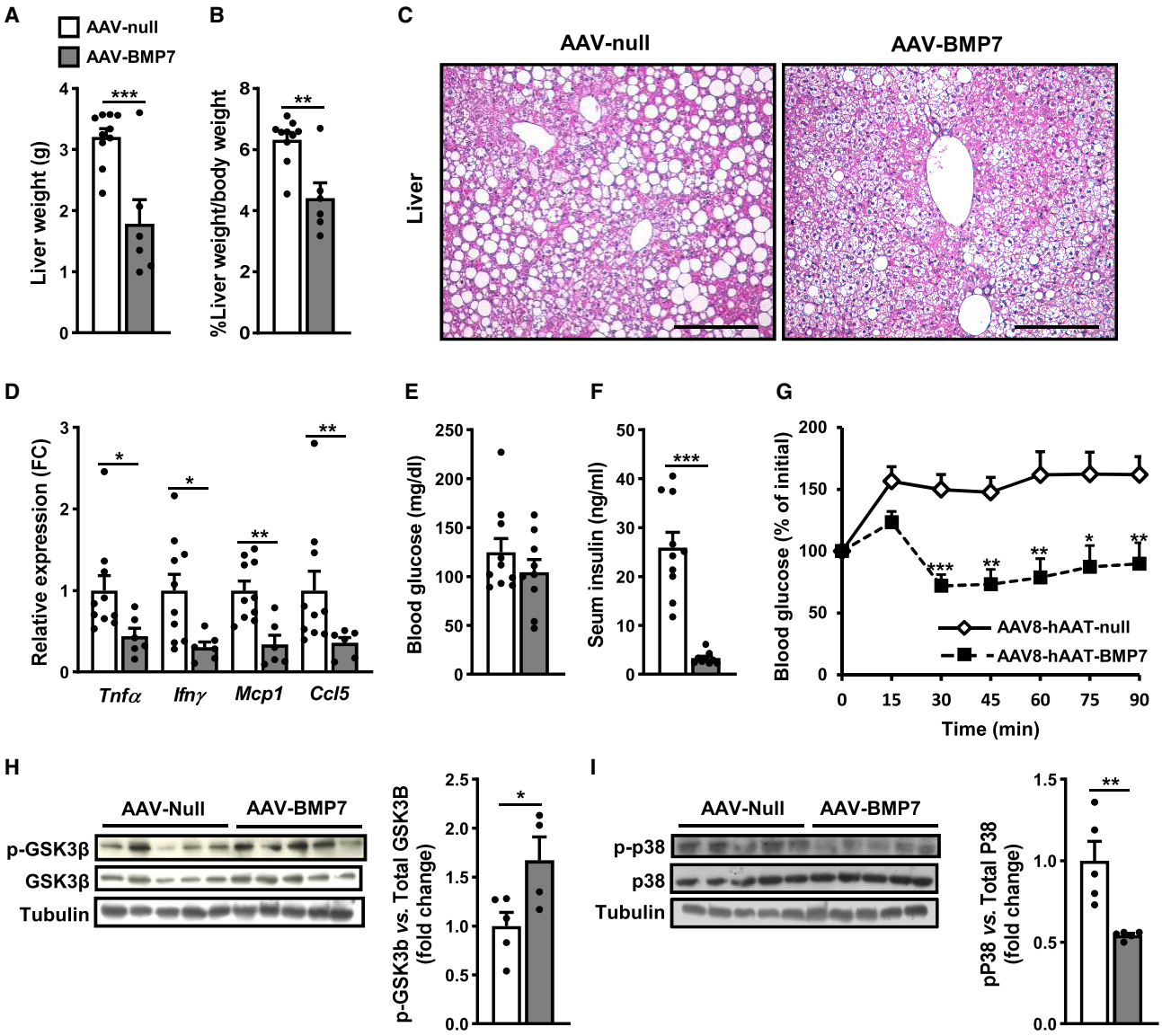

Figure 6. Improved insulin sensitivity in ob/ob mice treated with AAV-BMP7 vectors

(A) Liver weight (n = 6–10/group). (B) Liver weight normalized by body weight (n = 6–10/group). (C) Representative images of the hematoxylin-eosin staining of liver tissue sections obtained from ob/ob animals injected with either null or BMP7-encoding AAV. Scale bars: 200 μm. (D) Quantitative PCR analysis of the expression of the pro-inflammatory cytokines *Tnfα*, *Ifnγ*, *Mcp1*, and *Ccl5* in liver (n = 6–10/group). (E) Fed blood glucose levels at 5 weeks after vector administration (n = 9–10/group). (F) Fed serum insulin levels at 6 weeks after vector administration (n = 9–10/group). (G) Insulin tolerance test after intraperitoneal injection of insulin at a dose of 0.75 units insulin/kg body weight. Results were calculated as the percentage of initial blood glucose levels (n = 10, AAV-null, and n = 6, AAV-BMP7). (H) Determination of phosphorylated GSK3β (p-GSK3β) protein abundance in the liver: immunoblot and densitometric analysis (n = 4–5/group). (I) Determination of phosphorylated p38 (p-p38) protein abundance in the liver: immunoblot and densitometric analysis (n = 5/group). All values are expressed as the mean ± SEM. *p < 0.05, **p < 0.01, and ***p < 0.001.

mice. These results suggest that in obesity and insulin resistance conditions BMP7 resistance would not develop.

The effect of AAV-BMP7 on body weight loss in ob/ob mice may also be in part due to a decrease in food intake. Similar results were observed in HFD-fed and ob/ob mice treated with Ad-BMP7.[18] In this regard, BMP7 has been described as an anorectic factor, acting through leptin-independent mTOR pathways in the hypothalamus to reduce appetite.[18] In contrast, although HFD-fed mice treated with AAV-BMP7 showed lower food intake, when this parameter was normalized per body weight, these mice actually ate more than chow-fed mice. In the Ad-BMP7 study,[18] food intake data corrected by body weight are missing. Moreover, Ad-derived BMP7 serum levels were higher than in AAV-BMP7-treated HFD-fed mice but

similar to those exhibited by ob/ob mice treated with AAV-BMP7 vectors,[18] suggesting that BMP7 may exert anorectic effects only at very high circulating levels.

Non-alcoholic fatty liver disease (NAFLD) and NASH are strongly associated with insulin resistance and T2D.[72] In the present work, HFD-fed AAV-null-treated mice exhibited increased liver weight and hepatic lipid content, as well as marked inflammation. AAV-BMP7-treated HFD-fed and ob/ob mice animals showed counteraction of liver steatosis and inflammation, as also observed using recombinant BMP7 or Ad-BMP7 vectors.[17,18] Adiponectin is a key insulin-sensitizing and anti-inflammatory adipokine and is also associated with decreased hepatic steatosis.[73–75] Improvement of insulin sensitivity in ob/ob and HFD-fed mice overexpressing *Bmp7* in the liver could be mediated, at least in part, by increased circulating adiponectin levels. In humans, adiponectin levels are inversely correlated with the development of non-alcoholic fatty liver disease and with the degree of insulin resistance and T2D.[76,77] Treatment of HFD-fed mice and rats with recombinant adiponectin or gene transfer of adiponectin using AAV vectors decreased hepatic steatosis and increased insulin sensitivity.[74,75,78,79] Similarly, the increased circulating adiponectin levels in AAV-treated ob/ob and HFD-fed mice overexpressing *Bmp7* in the liver may play an important role in the amelioration of liver and WAT inflammation, thus contributing to reduced liver steatosis, which would in turn improve insulin sensitivity.

Recently, we have also demonstrated sustained amelioration of insulin sensitivity in ob/ob mice upon specific genetic engineering of WAT with BMP7-encoding AAV vectors, which resulted in increased but low levels of BMP7 in the bloodstream[15] compared with the circulating BMP7 levels observed in the present study or studies using Ad-BMP7 vectors.[16,18] In our previous study, AAV-mediated gene transfer of *Bmp7* to WAT of ob/ob mice induced white adipogenesis, which led to increased body weight but amelioration of insulin resistance.[15] In contrast, in the same study, treatment of ob/ob mice with 5×10^{11} vg of liver-directed AAV8-hAAT-BMP7 vector per mouse did not change adipogenesis despite similar low BMP7 circulating levels.[15] This was consistent with BMP7-mediated induction of hyperplasic expansion of WAT in an autocrine/paracrine manner. Altogether, these results suggest that BMP7 may elicit different effects depending on the circulating levels and site of production. Moreover, these studies highlight the need of high levels of circulating BMP7 to mediate whole-body correction of fat-derived metabolic alterations and normalization of body weight and insulin resistance in obese mice.

In summary, all these results demonstrate the relevance of the liver-directed AAV-BMP7-mediated gene therapy approach for the treatment of obesity and T2D. In this regard, AAV vectors have been used in clinical trials since the mid-1990s, and no adverse events related to these vectors have been described so far.[22,23] More than 3,000 patients have been enrolled in these studies and administered recombinant AAV vectors at different doses and through different routes to target several organs, mainly liver, skeletal muscle, brain, and eye.[22,23] Indeed, three of the seven gene therapy treatments approved for commercialization are AAV-based therapies.[23] Given that almost all natural AAV capsids can transduce liver efficiently following systemic administration,[23] AAV vectors provide a robust liver-targeting platform to treat a variety of diseases. In this regard, a total of 30 clinical trials for liver-directed AAV-mediated gene therapy to treat rare metabolic conditions in lean patients are currently ongoing.[80] It is also worth mentioning that BMP7 protein has already been approved by the FDA for the treatment of bone diseases.[14] Hence, the gene therapy strategy developed in this work may be envisaged as a novel approach for the future treatment of T2D and obesity.

MATERIALS AND METHODS

Animals

Eight-week-old male C57BL/6J littermate mice and 11-week-old male B6.V-*Lep*^{ob}/OlaHsd (ob/ob) littermate mice obtained from Envigo RMS SL (Spain) were used. Mice were kept in a specific-pathogen-free facility (SER-CBATEG, UAB) and maintained under a light-dark cycle of 12 h at 22°C. Mice were fed *ad libitum* with a standard diet (standard chow diet, Harlan Teklad Global Diet 2018, Envigo) or an HFD (TD.88137 Harlan Teklad). The HFD contained 15.2% protein, 42.7% carbohydrate, and 42% fat. The exact formula of the HFD included casein 195.0 g/kg, DL-methionine 3.0 g/kg, sucrose 341.46 g/kg, corn starch 150.0 g/kg, anhydrous milk fat 210.0 g/kg, cholesterol 1.5 g/kg, cellulose 50.0 g/kg, mineral mix AIN-76 (170915) 35.0 g/kg, calcium carbonate 4.0 g/kg, vitamin mix Teklad (40060) 10.0 g/kg, and ethoxyquin 0.04 g/kg. When stated, mice were fasted for 16 h. For tissue sampling, mice were anesthetized with inhalational anesthetic isoflurane (IsoFlo, Abbott Laboratories, Abbott Park, IL, USA) and decapitated. Tissues of interest were excised and kept at −80°C or in formalin until analysis. Animal care and experimental procedures were approved by the Ethics Committee in Animal and Human Experimentation of the Universitat Autònoma de Barcelona.

Recombinant AAV vectors

The AAV expression cassette was obtained by cloning, between the inverted terminal repeats (ITRs) of AAV2, an optimized murine *Bmp7* coding sequence (om*Bmp7*) under the control of a synthetic hybrid liver-specific promoter composed of three copies of the HCR enhancer from ApoE and the hAAT promoter (AAV-BMP7) A non-coding cassette carrying the synthetic HCR/hAAT promoter, but no transgene, was used to produce null vectors (AAV-null). Single-stranded AAV vectors of serotype 8 vectors were produced by triple transfection in HEK293 cells and purified using an optimized CsCl gradient-based purification protocol that renders vector preparations of high purity and devoid of empty capsids.[81] Viral genome titers were determined by PicoGreen using phage lambda DNA as the standard curve.

Administration of AAV vectors

For systemic administration, AAV vectors were diluted in 200 μL of 0.001% F68 Pluronic (Gibco) in PBS and injected via the tail vein. HFD-fed animals were injected with 1×10^{12} vg/animal. ob/ob mice were administered 1×10^{12} vg/animal.

Immunohistochemistry

Tissues were fixed for 12–24 h in 10% formalin, embedded in paraffin, and sectioned. Sections were incubated overnight at 4°C with rat anti-Mac2 (CL8942AP; Cedarlane). Biotinylated rabbit anti-rat (E0467; Dako) was used as secondary antibody. The ABC peroxidase kit (Pierce) was used for immunodetection, and sections were counterstained in Mayer's hematoxylin.

Measurement of the adipocyte area

A morphometric study of adipocyte size was performed in WAT sections stained with hematoxylin-eosin. Adipocyte area was determined as previously described.[82] A minimum of seven animals per group were used and at least 250 adipocytes per animal were analyzed.

RNA analysis

Total RNA was obtained from different tissues using an isolation reagent (Tripure, Roche, for liver and QIAzol, Qiagen, for adipose depots) and an RNeasy Minikit (Qiagen) and treated with DNase I (Qiagen). One microgram of total RNA was used for cDNA synthesis with the Transcriptor First Strand cDNA synthesis kit (Roche Diagnostics) using a combination of anchored-oligo(dT)18 and random hexamer priming at 55°C for 30 min according to the manufacturer's instructions. For gene expression quantification, retrotranscribed samples were diluted 1/10 and then 2 μL was used in triplicate qPCRs. Primers were used at a final concentration of 200 nM. Real-time qPCR was performed in a LightCycler 480 II (Roche) using the LightCycler 480 SyBr Green I Master Mix (Roche). Manufacturer standard cycling conditions were used: 10 s at 95°C, 10 s at 90°C, 10 s at 95°C for 45 cycles. Melting curve analysis was performed for each amplification to assess single product amplification. Data were normalized to *Rplp0* expression. After normalization, relative expression was calculated using the $2(-\Delta\Delta C(T))$ method.[83] omBmp7 gene expression was calculated after Rplp0 normalization and reported as arbitrary units, since it was not possible to perform relative quantification. The following *Mus musculus* primers were used: *omBmp7*, 5′-AGAGCATCAACCCTAAGCTGG-3′, 5′-TGTTCTGGGATCTCTGCTTGC-3′; endogenous *Bmp7*, 5′-TACATGAACGCCACCAACCA-3′, 5′-ACAGAGATGGCGTTGAGCTG-3′; *Ppargc1a*, 5′-ATACCGCAAAGAGCACGAGAAG-3′, 5′-CTCAAGAGCAGCGAAAGCGTCACAG-3′; *Ucp1*, 5′-GGATTGGCCTCTACGACTCAG-3′, 5′-TGTAGGCTGCCCAATGAACA-3′; *Cidea*, 5′-CCTACGACATCCGATGCACA-3′, 5′-GTATGTGCCCGCATAGACCA-3′; *Dio2*, 5′-AATTATGCCTCGGAGAAGACCG-3′, 5′-GGCAGTTGCCTAGTGAAAGGT-3′; *Elovl3*, 5′-GGACTTAAGGCCCTTTTTGG-3′, 5′-CCAACAACGATGAGCAACAG-3′; *Glut4*, 5′-TGCCCGAAAGAGTCTAAAGC-3′, 5′-TCCGTTTCTCATCCTTCAGC; *F4/80*, 5′-CTTTGGCTATGGGCTTCCAGTC-3′, 5′-GCAAGGAGGACAGAGTTTATC-3′; *Cd68*, 5′-GGGGCTCTTGGGAACTACAC-3′, 5′-CAAGCCCTCTTTAAGCCCCA-3′; *Mcp1*, 5′-AACTGCATCTGCCCTAAGGTC-3′, 5′-AAGTGCTTGAGGTGGTTGTG; *Tnfα*, 5′-CTGTAGCCCACGTCGTAGC-3′, 5′-TTGAGATCCATGCCGTTG-3′; *Ccl5*, 5′-GTGCCCACGTCAAGGAGTATT-3′, 5′-CCCACTTCTTCTCTGGGTTGG-3′; *Ifnγ*, 5′-AGACAATCAGGCCATCAGCA, 5′-TGGACCTGTGGGTTGTTGAC-3′; *Rplp0*, 5′-TCCCACCTTGTCTCCAGTCT-3′, 5′-ACTGGTCTAGGACCCGAGAAG-3′.

Vector genome copy number

Tissue samples were digested overnight at 56 °C in 300 μL of tissue lysis solution supplemented with proteinase K (0.2 mg/mL). Total DNA was isolated from supernatants with the MasterPure DNA purification kit (Lucigen). DNA was resuspended in distilled water and quantified using a NanoDrop ND-1000 spectrophotometer (NanoDrop). Vector genome copy number in 20 ng of total DNA was determined by quantitative PCR using LightCycler 480 Probes Master (Roche). Primers and probes were designed for a specific sequence within the SV40 poly(A) cDNA: forward primer, 5′-AGCAATAGCATCACAAATTTCACAA-3′; reverse primer, 5′-CAGACATGATAAGATACATTGATGAGTT-3′; probe, /56-FAM/AGCATTTTTTT/ZEN/CACTGCATTCTAGTTGTGGTTTGTC/3IABkFQ/. A reference standard curve was built from serial dilutions of a linearized plasmid bearing the hAAT promoter and the optimized *Bmp7* cDNA spiked into 20 ng/μL non-transduced mouse genomic DNA.

Western blot analysis

eWAT and liver samples were homogenized in protein lysis buffer. Proteins were separated by 12% SDS-PAGE and analyzed by immunoblotting with anti-P38 (#9212; Cell Signaling), anti-P38-P (#9211; Cell Signaling), anti-SMAD1 (#6944; Cell Signaling), anti-SMAD1/5/8-P (#13820; Cell Signaling), anti-GSK3β (#12456; Cell Signaling), and anti-GSK3β-P (#5558; Cell Signaling) antibodies. Detection was performed using ECL Plus detection reagent (Amersham Biosciences).

Hormone and metabolite assays

Hepatic triglyceride content was determined by chloroform:methanol (2:1 vol/vol) extraction of total lipids, as described previously.[84] Hepatic triglycerides and serum cholesterol were quantified spectrophotometrically using an enzymatic assay (Horiba-ABX) in a Pentra 400 analyzer (Horiba-ABX). Glycemia was determined using a Glucometer Elite (Bayer) and insulin levels were measured using the Rat Insulin ELISA kit (90010; Crystal Chem). Serum and liver BMP7 were determined using the Human BMP7 ELISA (DBP700; R&D Systems). The standard curve was conducted with the recombinant human BMP7 provided in the kit. The detection limit specified in the product datasheet was 31.3 pg/mL. Adiponectin and leptin were determined using the Mouse Adiponectin ELISA kit (80569; Crystal Chem) and the Mouse Leptin ELISA kit (90030; Crystal Chem), respectively.

Insulin tolerance test

Insulin (Humulin Regular; Eli Lilly) was injected intraperitoneally at a dose of 0.75 IU/kg body weight to fed mice. Glycemia was measured in tail vein blood samples at the indicated time points.

Glucose tolerance test

Awake mice were fasted overnight (16 h) and administered an intraperitoneal injection of glucose (1 g/kg body weight). Glycemia was measured in tail vein blood samples at the indicated time points.

Indirect calorimetry

An indirect open circuit calorimeter (Oxylet; Panlab) was used to monitor O_2 consumption and CO_2 production. Mice were individualized and acclimated to the metabolic chambers for 24 h. O_2 consumption and CO_2 production data were collected in each cage for 3 min, every 15 min, for 24 h during the light and dark cycles and adjusted by body weight. Activity was recorded continuously for 24 h during the light and dark cycles.

Statistical analysis

Sample size determination was based on previous experience with similar studies. Randomization was performed using the Excel function Roundup() or by GraphPad QuickCalcs to allocate mice in each group. In addition, we tested that the mean body weight and the mean glycemia were statistically not different for each experimental group prior to assignment to diet and/or treatment groups. All tests (ITT, GTT, etc.) and measurements (for example, adipocyte area) were performed by investigators blinded to the treatment. All results are expressed as the mean ± SEM. The GraphPad Prism 7 software was used for statistical analyses. Data were analyzed by one-way ANOVA with Tukey's *post hoc* correction, except for those parameters involving comparison of only two experimental groups, in which case an unpaired Student's t test was used. Differences were considered significant when $p < 0.05$.

SUPPLEMENTAL INFORMATION

Supplemental information can be found online at https://doi.org/10.1016/j.omtm.2022.03.007.

ACKNOWLEDGMENTS

The authors thank Marta Moya, Maria Molas, Jennifer Barrero, Lídia Hernández, and Lorena Noya for technical assistance. This work was supported by grants from the Ministerio de Economía, Industria y Competitividad (MINECO), the Agencia Estatal de Investigación (AEI) and Fondo Europeo de Desarrollo Regional (FEDER, EU), the Programa Estatal de I+D+i Orientada a los Retos de la Sociedad (SAF2017-86266R), grant PID2020-113864RB-I00 funded by MCIN/AEI/10.13039/501100011033, and the Generalitat de Catalunya (2017 SGR 1508, ICREA Academia Award to F.B.), Spain, and the European Foundation for the Study of Diabetes (EFSD/MSD European Research Program on Novel Therapies for Type 2 Diabetes, 2013). V.J. was the recipient of a post-doctoral research fellowship from EFSD/Lilly. E.C., V.S., and C.M. each received a predoctoral fellowship from the Ministerio de Educación, Cultura y Deporte, J.R. from the Ministerio de Economía y Competitividad, and I.G. from Ministerio de Ciencia e Innovación, Spain. V.S. received a predoctoral fellowship from the Generalitat de Catalunya, Spain.

AUTHOR CONTRIBUTIONS

E.C., V.J., and F.B. designed and supervised experiments, analyzed data, contributed to discussion, and wrote and edited the manuscript. E.C., V.J., C.J., V.S., S.M., J.R., M.G., I.G., and C.M. generated reagents and performed experiments. X.L. produced AAV vectors. A.C., V.S., T.F., and S.M. performed experiments. S.F. contributed to discussion.

DECLARATION OF INTERESTS

The authors declare no competing interests.

REFERENCES

1. Duclos, M. (2016). Osteoarthritis, obesity and type 2 diabetes: the weight of waist circumference. Ann. Phys. Rehabil. Med. *59*, 157–160.
2. Van Gaal, L.F., Mertens, I.L., and De Block, C.E. (2006). Mechanisms linking obesity with cardiovascular disease. Nature *444*, 875–880.
3. Renehan, A.G., Tyson, M., Egger, M., Heller, R.F., and Zwahlen, M. (2008). Body-mass index and incidence of cancer: a systematic review and meta-analysis of prospective observational studies. Lancet *371*, 569–578.
4. Kim, B., and Feldman, E.L. (2015). Insulin resistance as a key link for the increased risk of cognitive impairment in the metabolic syndrome. Exp. Mol. Med. *47*, e149.
5. Association, A.D. (2018). Classification and diagnosis of diabetes: standards of medical care in Diabetesd2018. Diabetes Care *41*, S13–S27.
6. van Marken Lichtenbelt, W.D., Vanhommerig, J.W., Smulders, N.M., Drossaerts, J.M., Kemerink, G.J., Bouvy, N.D., Schrauwen, P., and Teule, G.J. (2009). Cold-activated brown adipose tissue in healthy men. N. Engl. J. Med. *360*, 1500–1508.
7. Cypess, A.M., Lehman, S., Williams, G., Tal, I., Rodman, D., Goldfine, A.B., Kuo, F.C., Palmer, E.L., Tseng, Y.-H., Doria, A., et al. (2009). Identification and importance of Brown adipose tissue in adult humans. N. Engl. J. Med. *360*, 1509–1517.
8. Zhang, Z., Zhang, H., Li, B., Meng, X., Wang, J., Zhang, Y., Yao, S., Ma, Q., Jin, L., Yang, J., et al. (2014). Berberine activates thermogenesis in white and brown adipose tissue. Nat. Commun. *5*, 1–15.
9. Yin, N., Zhang, H., Ye, R., Dong, M., Lin, J., Zhou, H., Huang, Y., Chen, L., Jiang, X., Nagaoka, K., et al. (2019). Fluvastatin sodium ameliorates obesity through brown fat activation. Int. J. Mol. Sci. *20*, 1622. https://doi.org/10.3390/ijms20071622.
10. Lee, P., Swarbrick, M.M., and Ho, K.K.Y. (2013). Brown adipose tissue in adult humans: a metabolic renaissance. Endocr. Rev. *34*, 413–438.
11. Lee, P., Greenfield, J.R., Ho, K.K.Y., and Fulham, M.J. (2010). A critical appraisal of the prevalence and metabolic significance of brown adipose tissue in adult humans. Am. J. Physiol. - Endocrinol. Metab. *299*, E601–E606. https://doi.org/10.1152/ajpendo.00298.2010.
12. Thamer, C., Machann, J., Staiger, H., Müssig, K., Schwenzer, N., Ludescher, B., Machicao, F., Claussen, C., Fritsche, A., Schick, F., et al. (2010). Interscapular fat is strongly associated with insulin resistance. J. Clin. Endocrinol. Metab. *95*, 4736–4742.
13. Oxburgh, L. (2009). Control of the bone morphogenetic protein 7 gene in developmental and adult life. Curr. Genomics *10*, 223–230.
14. Carreira, A.C.O., Zambuzzi, W.F., Rossi, M.C., Filho, R.A., Sogayar, M.C., and Granjeiro, J.M. (2015). Bone morphogenetic proteins: promising molecules for bone healing, bioengineering, and regenerative medicine. In The Bone Morphogenetic Proteins and Their Antagonists. Vitamins and Hormones, *99*, Gerald Litwack, ed (Elsevier Inc.), pp. 293–322.
15. Casana, E., Jimenez, V., Sacristan, V., Muñoz, S., Jambrina, C., Rodó, J., et al. (2021). BMP7 overexpression in adipose tissue induces white adipogenesis and improves insulin sensitivity in ob/ob mice. Int. J. Obes. 449–460.
16. Tseng, Y.-H., Kokkotou, E., Schulz, T.J., Huang, T.L., Winnay, J.N., Taniguchi, C.M., Tran, T.T., Suzuki, R., Espinoza, D.O., Yamamoto, Y., et al. (2008). New role of bone morphogenetic protein 7 in brown adipogenesis and energy expenditure. Nature *454*, 1000–1004.
17. Boon, M.R., van den Berg, S.A.A., Wang, Y., van den Bossche, J., Karkampouna, S., Bauwens, M., De Saint-Hubert, M., van der Horst, G., Vukicevic, S., de Winther, M.P.J., et al. (2013). BMP7 activates Brown adipose tissue and reduces diet-induced obesity only at subthermoneutrality. PLoS One *8*, e74083.
18. Townsend, K.L., Suzuki, R., Huang, T.L., Jing, E., Schulz, T.J., Lee, K., Taniguchi, C.M., Espinoza, D.O., McDougall, L.E., Zhang, H., et al. (2012). Bone morphogenetic protein 7 (BMP7) reverses obesity and regulates appetite through a central mTOR pathway. FASEB J. *7*, 1–10.
19. Chattopadhyay, T., Singh, R.R., Gupta, S., and Surolia, A. (2017). Bone morphogenetic protein-7 (BMP-7) augments insulin sensitivity in mice with type II diabetes mellitus by potentiating PI3K/AKT pathway. BioFactors *43*, 195–209.

20. Romano, G. (2006). The controversial role of adenoviral-derived vectors in gene therapy programs: where do we stand? Drug News Perspect. *19*, 99.

21. Descamps, D., and Benihoud, K. (2009). Two key challenges for effective adenovirus-mediated liver gene therapy:innate immune responses and hepatocyte-specific transduction. Curr. Gene Ther. *9*, 115–127.

22. Kuzmin, D.A., Shutova, M.V., Johnston, N.R., Smith, O.P., Fedorin, V.V., Kukushkin, Y.S., van der Loo, J.C.M., and Johnstone, E.C. (2021). The clinical landscape for AAV gene therapies. Nat. Rev. Drug Discov. *20*, 173–174.

23. Mendell, J.R., Al-Zaidy, S.A., Rodino-Klapac, L.R., Goodspeed, K., Gray, S.J., Kay, C.N., Boye, S.L., Boye, S.E., George, L.A., Salabarria, S., et al. (2021). Current clinical applications of in vivo gene therapy with AAVs. Mol. Ther. *29*, 464–488.

24. Petanceska, S.S., DeRosa, S., Sharma, A., Diaz, N., Duff, K., Tint, S.G., Refolo, L.M., and Pappolla, M. (2003). Changes in apolipoprotein E expression in response to dietary and pharmacological modulation of cholesterol. J. Mol. Neurosci. *20*, 395–406.

25. Lin-Lee, Y.C., Tanaka, Y., Lin, C.T., and Chan, L. (1981). Effects of an atherogenic diet on apolipoprotein E biosynthesis in the rat. Biochemistry *20*, 6474–6480.

26. Driscoll, D.M., Mazzone, T., Matsushima, T., and Getz, G.S. (1990). Apoprotein E biosynthesis in the cholesterol-fed Guinea pig. Arteriosclerosis *10*, 31–39.

27. Garcia, R.E., Beck, D.L., Wright, D.A., Tomlinson, J.E., Nakayama, R., and Holten, D. (1984). Effect of dietary cholesterol on apolipoprotein E synthesis in the rabbit. Atherosclerosis *51*, 199–210.

28. Li, Y., Zou, S., Ding, H., Hao, N., Huang, Y., Tang, J., Cheng, J., Feng, S., Li, J., Wang, X., et al. (2020). Low expression of sirtuin 1 in the dairy cows with mild fatty liver alters hepatic lipid metabolism. Anim. Open Access J. MDPI *10*, 560.

29. Özkaynak, E., Schnegelsberg, P.N.J., and Oppermann, H. (1991). Murine osteogenic protein (OP-1): high levels of mRNA in kidney. Biochem. Biophys. Res. Commun. *179*, 116–123.

30. Hajer, G.R., van Haeften, T.W., and Visseren, F.L.J. (2008). Adipose tissue dysfunction in obesity, diabetes, and vascular diseases. Eur. Heart J. *29*, 2959–2971.

31. Townsend, K.L., An, D., Lynes, M.D., Huang, T.L., Zhang, H., Goodyear, L.J., and Tseng, Y.H. (2013). Increased mitochondrial activity in BMP7-treated brown adipocytes, due to increased CPT1-and CD36-mediated fatty acid uptake. Antioxid. Redox Signal *19*, 243–257.

32. Lee, M.J. (2018). Transforming growth factor beta superfamily regulation of adipose tissue biology in obesity. Biochim. Biophys. Acta. Mol. Basis Dis. *1864*, 1160–1171.

33. Fellmann, L., Nascimento, A.R., Tibiriça, E., and Bousquet, P. (2013). Murine models for pharmacological studies of the metabolic syndrome. Pharmacol. Ther. *137*, 331–340.

34. Ma, H., Yuan, J., Ma, J., Ding, J., Lin, W., Wang, X., Zhang, M., Sun, Y., Wu, R., Liu, C., et al. (2019). BMP7 improves insulin signal transduction in the liver via inhibition of mitogen-activated protein kinases. J. Endocrinol. *243*, 97–110.

35. Fuchs, T., Loureiro, M. de P., Macedo, L.E., Nocca, D., Nedelcu, M., and Costa-Casagrande, T.A. (2018). Animal models in metabolic syndrome. Rev. Col. Bras. Cir. *45*, e1975.

36. Davidoff, A.M., Ng, C.Y.C., Zhou, J., Spence, Y., and Nathwani, A.C. (2003). Sex significantly influences transduction of murine liver by recombinant adeno-associated viral vectors through an androgen-dependent pathway. Blood *102*, 480–488.

37. Ruzo, A., Garcia, M., Ribera, A., Villacampa, P., Haurigot, V., Marcó, S., Ayuso, E., Anguela, X.M., Roca, C., Agudo, J., et al. (2012). Liver production of sulfamidase reverses peripheral and ameliorates CNS pathology in mucopolysaccharidosis IIIA mice. Mol. Ther. *20*, 254–266.

38. Ribera, A., Haurigot, V., Garcia, M., Marcó, S., Motas, S., Villacampa, P., Maggioni, L., León, X., Molas, M., Sánchez, V., et al. (2015). Biochemical, histological and functional correction of mucopolysaccharidosis type IIIB by intra-cerebrospinal fluid gene therapy. Hum. Mol. Genet. *24*, 2078–2095.

39. Guenzel, A.J., Collard, R., Kraus, J.P., Matern, D., and Barry, M.A. (2015). Long-term sex-biased correction of circulating propionic acidemia disease markers by adeno-associated virus vectors. Hum. Gene Ther. *26*, 153–160.

40. Pañeda, A., Vanrell, L., Mauleon, I., Crettaz, J.S., Berraondo, P., Timmermans, E.J., Beattie, S.G., Twisk, J., Van Deventer, S., Prieto, J., et al. (2009). Effect of adeno-associated virus serotype and genomic structure on liver transduction and biodistribution in mice of both genders. Hum. Gene Ther. *20*, 908–917.

41. Ruzo, A., Marcó, S., García, M., Villacampa, P., Ribera, A., Ayuso, E., Maggioni, L., Mingozzi, F., Haurigot, V., and Bosch, F. (2012). Correction of pathological accumulation of glycosaminoglycans in central nervous system and peripheral tissues of MPSIIIA mice through systemic AAV9 gene transfer. Hum. Gene Ther. *23*, 1237–1246.

42. Haurigot, V., Marcó, S., Ribera, A., Garcia, M., Ruzo, A., Villacampa, P., Ayuso, E., Añor, S., Andaluz, A., Pineda, M., et al. (2013). Whole body correction of mucopolysaccharidosis IIIA by intracerebrospinal fluid gene therapy. J. Clin. Invest. *123*, 3254–3271.

43. Nathwani, A.C., Cochrane, M., McIntosh, J., Ng, C.Y.C., Zhou, J., Gray, J.T., and Davidoff, A.M. (2009). Enhancing transduction of the liver by adeno-associated viral vectors. Gene Ther. *16*, 60–69.

44. Berraondo, P., Crettaz, J., Ochoa, L., Pañeda, A., Prieto, J., Trocóniz, I.F., and González-Aseguinolaza, G. (2006). Intrahepatic injection of recombinant adeno-associated virus serotype 2 overcomes gender-related differences in liver transduction. Hum. Gene Ther. *17*, 601–610.

45. Wang, L., and Herzog, R. (2005). AAV-mediated gene transfer for treatment of hemophilia. Curr. Gene Ther. *5*, 349–360.

46. Ruzo, A., Marcó, S., García, M., Villacampa, P., Ribera, A., Ayuso, E., Maggioni, L., Mingozzi, F., Haurigot, V., and Bosch, F. (2012). Correction of pathological accumulation of glycosaminoglycans in central nervous system and peripheral tissues of MPSIIIA mice through systemic AAV9 gene transfer. Hum. Gene Ther. *23*, 1237–1246.

47. Binny, C., McIntosh, J., Della Peruta, M., Kymalainen, H., Tuddenham, E.G.D., Buckley, S.M.K., Waddington, S.N., McVey, J.H., Spence, Y., Morton, C.L., et al. (2012). AAV-mediated gene transfer in the perinatal period results in expression of FVII at levels that protect against fatal spontaneous hemorrhage. Blood *119*, 957–966.

48. Greig, J.A., Limberis, M.P., Bell, P., Chen, S.J., Calcedo, R., Rader, D.J., and Wilson, J.M. (2017). Non-clinical study examining AAV8.TBG.hLDLR vector-associated toxicity in chow-fed wild-type and LDLR +/- rhesus macaques. Hum. Gene Ther. Clin. Dev. *28*, 39–50.

49. Jimenez, V., Jambrina, C., Casana, E., Sacristan, V., Muñoz, S., Darriba, S., Rodó, J., Mallol, C., Garcia, M., León, X., et al. (2018). FGF21 gene therapy as treatment for obesity and insulin resistance. EMBO Mol. Med. *10*, e8791.

50. Shaw, A., Tóth, B.B., Arianti, R., Csomós, I., Póliska, S., Vámos, A., Bacso, Z., Győry, F., Fésüs, L., and Kristóf, E. (2021). Bmp7 increases ucp1-dependent and independent thermogenesis with a unique gene expression program in human neck area derived adipocytes. Pharmaceuticals *14*, 1078.

51. Schulz, T.J., Huang, T.L., Tran, T.T., Zhang, H., Townsend, K.L., Shadrach, J.L., Cerletti, M., McDougall, L.E., Giorgadze, N., Tchkonia, T., et al. (2011). Identification of inducible brown adipocyte progenitors residing in skeletal muscle and white fat. Proc. Natl. Acad. Sci. U S A *108*, 143–148.

52. Okla, M., Ha, J.H., Temel, R.E., and Chung, S. (2015). BMP7 drives human adipogenic stem cells into metabolically active beige adipocytes. Lipids *50*, 111–120.

53. Ferrannini, G., Namwanje, M., Fang, B., Damle, M., Li, D., Liu, Q., Lazar, M.A., and Qiang, L. (2016). Genetic backgrounds determine brown remodeling of white fat in rodents. Mol. Metab. *5*, 948–958.

54. Liu, B., Page, A.J., Hutchison, A.T., Wittert, G.A., and Heilbronn, L.K. (2019). Intermittent fasting increases energy expenditure and promotes adipose tissue browning in mice. Nutrition *66*, 38–43.

55. Kim, Y.H., Lee, J.H., Yeung, J.L.-H., Das, E., Kim, R.Y., Jiang, Y., Moon, J.H., Jeong, H., Thakkar, N., Son, J.E., et al. (2019). Thermogenesis-independent metabolic benefits conferred by isocaloric intermittent fasting in ob/ob mice. Sci. Rep. *9*, 2479.

56. Li, G., Xie, C., Lu, S., Nichols, R.G., Tian, Y., Li, L., Patel, D., Ma, Y., Brocker, C.N., Yan, T., et al. (2017). Intermittent fasting promotes white adipose browning and decreases obesity by shaping the gut microbiota. Cell Metab *26*, 672–685.e4.

57. Collins, S., Daniel, K.W., Petro, A.E., and Surwit, R.S. (1997). Strain-specific response toβ_3-adrenergic receptor agonist treatment of diet-induced obesity in mice [1]. Endocrinology *138*, 405–413.

58. Guerra, C., Koza, R.A., Yamashita, H., Walsh, K., and Kozak, L.P. (1998). Emergence of brown adipocytes in white fat in mice is under genetic control effects on body weight and adiposity. J. Clin. Invest. *102*, 412–420.

59. Cypess, A.M., Lehman, S., Williams, G., Tal, I., Rodman, D., Goldfine, A.B., Kuo, F.C., Palmer, E.L., Tseng, Y.-H., Doria, A., et al. (2009). Identification and importance of Brown adipose tissue in adult humans. N. Engl. J. Med. *360*, 1509–1517.

60. Jespersen, N.Z., Larsen, T.J., Peijs, L., Daugaard, S., Homøe, P., Loft, A., De Jong, J., Mathur, N., Cannon, B., Nedergaard, J., et al. (2013). A classical brown adipose tissue mrna signature partly overlaps with brite in the supraclavicular region of adult humans. Cell Metab *17*, 798–805.

61. Lidell, M.E., Betz, M.J., and Enerbäck, S. (2014). Two types of brown adipose tissue in humans. Adipocyte *3*, 63–66.

62. Frontini, A., Vitali, A., Perugini, J., Murano, I., Romiti, C., Ricquier, D., Guerrieri, M., and Cinti, S. (2013). White-to-brown transdifferentiation of omental adipocytes in patients affected by pheochromocytoma. Biochim. Biophys. Acta *1831*, 950–959.

63. Li, S., Li, Y., Xiang, L., Dong, J., Liu, M., and Xiang, G. (2018). Sildenafil induces browning of subcutaneous white adipose tissue in overweight adults. Metabolism *78*, 106–117.

64. Sidossis, L.S., Porter, C., Saraf, M.K., Børsheim, E., Radhakrishnan, R.S., Chao, T., Ali, A., Chondronikola, M., Mlcak, R., Finnerty, C.C., et al. (2015). Browning of subcutaneous white adipose tissue in humans after severe adrenergic stress. Cell Metab. *22*, 219–227.

65. Hoffmann, J.M., Grünberg, J.R., Church, C., Elias, I., Palsdottir, V., Jansson, J.-O., Bosch, F., Hammarstedt, A., Hedjazifar, S., and Smith, U. (2017). BMP4 gene therapy in mature mice reduces BAT activation but protects from obesity by browning subcutaneous adipose tissue. Cell Rep. *20*, 1038–1049.

66. Hoffmann, J.M., Grünberg, J.R., Hammarstedt, A., Kroon, T., Greiner, T.U., Maurer, S., Elias, I., Palsdottir, V., Bosch, F., Boucher, J., et al. (2020). BMP4 gene therapy enhances insulin sensitivity but not adipose tissue browning in obese mice. Mol. Metab. *32*, 15–26.

67. Hoffmann, J.M., Grünberg, J.R., Hammarstedt, A., Kroon, T., Greiner, T.U., Maurer, S., Elias, I., Palsdottir, V., Bosch, F., Boucher, J., et al. (2020). BMP4 gene therapy enhances insulin sensitivity but not adipose tissue browning in obese mice. Mol. Metab. *32*, 15–26.

68. Gustafson, B., Hammarstedt, A., Hedjazifar, S., Hoffmann, J.M., Svensson, P.A., Grimsby, J., Rondinone, C., and Smith, U. (2015). BMP4 and BMP antagonists regulate human white and beige adipogenesis. Diabetes *64*, 1670–1681.

69. Son, J.W., Kim, M.K., Park, Y.M., Baek, K.H., Yoo, S.J., Song, K.H., Son, H.S., Yoon, K.H., Lee, W.C., Cha, B.Y., et al. (2011). Association of serum bone morphogenetic protein 4 levels with obesity and metabolic syndrome in non-diabetic individuals. Endocr. J. *58*, 39–46.

70. Modica, S., Straub, L.G., Balaz, M., Sun, W., Wolfrum, C., Varga, L., Ukropcova, B., Ukropec, J., Varga, L., Stefanicka, P., et al. (2016). Bmp4 promotes a Brown to white-like adipocyte shift. Cell Rep *16*, 2243–2258.

71. Wang, X., Chen, J., Li, L., Zhu, C.L., Gao, J., Rampersad, S., Bu, L., and Qu, S. (2017). New association of bone morphogenetic protein 4 concentrations with fat distribution in obesity and Exenatide intervention on it. Lipids Health Dis. *16*, 70.

72. Kitade, H., Chen, G., Ni, Y., and Ota, T. (2017). Nonalcoholic fatty liver disease and insulin resistance: new insights and potential new treatments. Nutrients *9*, 387.

73. Kim, J.Y., Van De Wall, E., Laplante, M., Azzara, A., Trujillo, M.E., Hofmann, S.M., Schraw, T., Durand, J.L., Li, H., Li, G., et al. (2007). Obesity-associated improvements in metabolic profile through expansion of adipose tissue. J. Clin. Invest. *117*, 2621–2637.

74. Shklyaev, S., Aslanidi, G., Tennant, M., Prima, V., Kohlbrenner, E., Kroutov, V., Campbell-Thompson, M., Crawford, J., Shek, E.W., Scarpace, P.J., et al. (2003). Sustained peripheral expression of transgene adiponectin offsets the development of diet-induced obesity in rats. Proc. Natl. Acad. Sci. U S A *100*, 14217–14222.

75. Long, W., Hui Ju, Z., Fan, Z., Jing, W., and Qiong, L. (2014). The effect of recombinant adeno-associated virus-adiponectin (rAAV2/1-Acrp30) on glycolipid dysmetabolism and liver morphology in diabetic rats. Gen. Comp. Endocrinol. *206*, 1–7.

76. Cnop, M., Havel, P.J., Utzschneider, K.M., Carr, D.B., Sinha, M.K., Boyko, E.J., Retzlaff, B.M., Knopp, R.H., Brunzell, J.D., and Kahn, S.E. (2003). Relationship of adiponectin to body fat distribution, insulin sensitivity and plasma lipoproteins: evidence for independent roles of age and sex. Diabetologia *46*, 459–469.

77. Ma, H., Gomez, V., Lu, L., Yang, X., Wu, X., and Xiao, S.Y. (2009). Expression of adiponectin and its receptors in livers of morbidly obese patients with non-alcoholic fatty liver disease. J. Gastroenterol. Hepatol. *24*, 233–237.

78. Xu, A., Wang, Y., Keshaw, H., Xu, L.Y., Lam, K.S.L., and Cooper, G.J.S. (2003). The fat-derived hormone adiponectin alleviates alcoholic and nonalcoholic fatty liver diseases in mice. J. Clin. Invest. *112*, 91–100.

79. Ma, H., Cui, F., Dong, J.-J., You, G.-P., Yang, X.-J., Lu, H.-D., and Huang, Y.-L. (2014). Therapeutic effects of globular adiponectin in diabetic rats with nonalcoholic fatty liver disease. World J. Gastroenterol. *20*, 14950–14957.

80. Piccolo, P., Rossi, A., and Brunetti-Pierri, N. (2021). Liver-directed gene-based therapies for inborn errors of metabolism. Expert Opin. Biol. Ther. *21*, 229–240.

81. Ayuso, E., Mingozzi, F., Montane, J., Leon, X., Anguela, X.M., Haurigot, V., Edmonson, S.A., Africa, L., Zhou, S., High, K.A., et al. (2010). High AAV vector purity results in serotype- and tissue-independent enhancement of transduction efficiency. Gene Ther. *17*, 503–510.

82. Muñoz, S., Franckhauser, S., Elias, I., Ferré, T., Hidalgo, A., Monteys, A.M., Molas, M., Cerdán, S., Pujol, A., Ruberte, J., et al. (2010). Chronically increased glucose uptake by adipose tissue leads to lactate production and improved insulin sensitivity rather than obesity in the mouse. Diabetologia *53*, 2417–2430.

83. Livak, K.J., and Schmittgen, T.D. (2001). Analysis of relative gene expression data using real-time quantitative PCR and the $2-\Delta\Delta CT$ method. Methods *25*, 402–408.

84. Carr, T.P., Andresen, C.J., and Rudel, L.L. (1993). Enzymatic determination of triglyceride, free cholesterol, and total cholesterol in tissue lipid extracts. Clin. Biochem. *26*, 39–42.